

# A Modified LU Recombination Technique for Improving the Performance of Boundary Element Methods at Low Frequencies

Haixin Ke and Todd H. Hubing  
Department of Electrical and Computer Engineering  
University of Missouri-Rolla  
Rolla, MO 65409

## ABSTRACT

Many numerical electromagnetic modeling techniques that work very well at high frequencies do not work well at lower frequencies. This is directly or indirectly due to the weak coupling between the electric and magnetic fields at low frequencies. One technique for improving the performance of boundary element techniques at low frequencies is through the use of loop-tree basis functions, which decouple the contributions from the vector and scalar electric potential. However, loop-tree basis functions can be difficult to define for large, complex geometries. This paper describes a method for improving the low-frequency performance of boundary element techniques that does not require the explicit definition of loop-tree basis functions. The method is a modified version of an LU recombination method proposed earlier. It automatically detects the linear space spanned by the scalar electric potential and corrects numerical errors during the LU decomposition of the impedance matrix. This method does not require special basis functions and is relatively easy to implement. Several examples are presented to demonstrate the effectiveness of this method.

## I. INTRODUCTION

The boundary element method is a widely used numerical electromagnetic modeling technique. Boundary element modeling codes use the method of moments to solve an electric field integral equation (EFIE) or magnetic field integral equation (MFIE) to calculate equivalent currents induced on a surface in the presence of an exciting field. There are many boundary element modeling codes available that do an excellent job of modeling complex geometries at high frequencies (megahertz and higher). At low frequencies however, these codes may exhibit instabilities, particularly when using general purpose basis functions such as the popular Rao-Wilton-Glisson (RWG) [1] basis functions [2, 3, 4]. These instabilities can be explained in terms of the natural Helmholtz decomposition of Maxwell's equations [5]. At low

frequencies, the magnetic vector potential and the electric scalar potential become more decoupled. Their representations in the impedance matrix become heavily imbalanced [3, 6, 7] and this imbalance results in the loss of important information due to the finite precision of the numerical computations.

Loop-tree basis functions have been proposed to overcome this difficulty [3]. These basis functions allow the divergence-free and the curl-free components of the current, which have different frequency dependencies, to be separated [5]. The round-off error due to the difference in size of the scalar and vector potential contributions is avoided. Unfortunately, loop-tree basis functions are not widely used because they can be difficult to work with; particularly if the geometry being modeled is large and complex.

In [8] an LU recombination method was proposed that mathematically forced the scalar potential to be zero around loops, without explicitly defining new basis functions. It was readily applied to existing moment method algorithms. This method works well for simple structures like small loops but does not model surface currents correctly on large plates.

In this paper we present a modified LU recombination method. This method extracts the linear dependence information from the  $\mathbf{L}$  matrix and modifies both the  $\mathbf{L}$  and  $\mathbf{U}$  matrices to remove the error in the linear relations and recover the space spanned by the scalar potentials. Examples show that this method works better than the previous LU recombination method.

The rest of the paper is organized as follows: Section II explains the reason for the low-frequency errors in boundary element codes and briefly describes loop-tree basis functions; Section III introduces the new method based on LU decomposition; Section IV presents several numerical examples; and finally in Section V, we provide a brief summary.

## II. LOW-FREQUENCY PROBLEM AND LOOP-TREE SCHEME

Consider the electromagnetic scattering from perfect electric conductors (PECs). The “mixed-potential” form of the scattered electric field is expressed as

$$\mathbf{E}^{sca} = -j\omega\mathbf{A} - \nabla\Phi. \quad (1)$$

The first term on the right-hand side of this equation is directly proportional to frequency while the second term is not. At low frequencies, the scalar potential term dominates.

The low frequency problem can be understood by examining the testing process [9]. A vector identity states that the integration of the gradient,  $\nabla\Phi$ , is path-independent. If the scatterer mesh allows current to flow in closed loops, the testing of the scalar potentials associated with the loops should cancel. If, due to numerical error, the testing of scalar potential is not exactly zero when evaluated around a closed loop, the error can overwhelm the vector potential term in (1) at low frequencies. The solution to the matrix equation then becomes unstable.

The construction of the loop-tree basis functions starts with the physical decomposition of current,

$$\mathbf{J} = \mathbf{J}^s + \mathbf{J}^i, \quad (2)$$

where  $\mathbf{J}^s$  is the solenoidal current and  $\mathbf{J}^i$  is the irrotational component. Loop basis functions are used to expand  $\mathbf{J}^s$  and tree basis functions to expand  $\mathbf{J}^i$ .

A loop basis function is associated with an inner node and its surrounding edges. Explicitly, the definition in terms of RWG basis functions is [2],

$$\mathbf{O}_n(\mathbf{r}) = \sum_{i \in \text{loop}_n} \frac{\sigma_i}{\lambda_i} \mathbf{f}_i(\mathbf{r}), \quad (3)$$

where  $\mathbf{f}_i$  is the RWG basis function for the  $i^{\text{th}}$  edge connected to node  $n$ .  $\lambda_i$  is the length of the edge and the coefficient  $\sigma_i = \pm 1$  forces the current to flow in the same direction around node  $n$ .

Tree basis functions are simply chosen from a subset of the RWG basis functions and are complementary to the loop basis functions. It is easy to show that the loop basis functions are divergence-free. Physically, that means there is no charge associated with the loop basis functions.

The loop-tree basis function scheme inherently forces the numerical integration of  $\nabla\Phi$  over closed paths to be exactly zero and preserves the

information contained in  $\mathbf{A}$ . However, to take advantage of this technique, one has to identify all possible closed paths in the mesh. This requires searching the mesh to locate the inner nodes, identifying shared edges for each inner node, and adjusting the basis functions associated with the edges to orient them properly. This procedure can be cumbersome [2].

## III. THE MODIFIED LU RECOMBINATION METHOD

The modified LU recombination method described here takes advantage of the fact that the loop-tree basis functions are linear combinations of the RWG basis functions. In this method, the reordering of the impedance matrix is performed automatically without having to identify current loops explicitly.

Consider the following  $N \times N$  matrix equation,

$$\mathbf{C} \cdot \mathbf{J} = \mathbf{F} \quad (4)$$

obtained after applying the method of moments using RWG basis and testing functions.  $\mathbf{J} = [J_n]$  is a vector of the unknown surface current densities which are normal to the edges.  $\mathbf{F} = [F_m]$  is the excitation vector.  $\mathbf{C} = [C_{mn}]$  is the  $N \times N$  impedance matrix. Each row of  $\mathbf{C}$  corresponds to an edge in the mesh. The elements of  $\mathbf{C}$  are given by [10],

$$\begin{aligned} C_{mn} &= C_{1mn} + C_{2mn} \\ &= jk\eta \int_{T_m} \mathbf{f}_m(\mathbf{r}) \cdot \left[ \int_{T_n} \mathbf{f}_n(\mathbf{r}') \mathbf{G}_0(\mathbf{r}, \mathbf{r}') dS' \right] dS \\ &\quad + j \frac{\eta}{k} \int_{T_m} \mathbf{f}_m(\mathbf{r}) \cdot \left[ \int_{T_n} (\nabla' \cdot \mathbf{f}_n(\mathbf{r}')) \nabla' \mathbf{G}_0(\mathbf{r}, \mathbf{r}') dS' \right] dS \end{aligned} \quad (5)$$

where  $k$  is the wave number and  $\eta$  the intrinsic impedance.  $\mathbf{C}_1$  is the vector potential component and  $\mathbf{C}_2$  is the scalar potential component of  $\mathbf{C}$ . The function  $\mathbf{f}_n$  is the RWG basis function defined on triangle pair  $T_n$ .  $T_n$  is composed of two triangles,  $T_n^+$  and  $T_n^-$ , sharing edge  $n$ .  $\mathbf{G}_0$  is the free space Green's function.  $\mathbf{r}$  and  $\mathbf{r}'$  are the observation and source points, respectively. We can write the elements of  $\mathbf{C}_2$ , the second integral on the right of (5), as

$$\begin{aligned} C_{2mn} &= j \frac{\eta}{k} \int_{T_m^+} (\nabla \cdot \mathbf{f}_m) \left[ \int_{T_n^+} (\nabla' \cdot \mathbf{f}_n) \mathbf{G}_0(\mathbf{r}, \mathbf{r}') dS' \right] dS \\ &\quad + j \frac{\eta}{k} \int_{T_m^-} (\nabla \cdot \mathbf{f}_m) \left[ \int_{T_n^-} (\nabla' \cdot \mathbf{f}_n) \mathbf{G}_0(\mathbf{r}, \mathbf{r}') dS' \right] dS \\ &\quad + j \frac{\eta}{k} \int_{T_m^+} (\nabla \cdot \mathbf{f}_m) \left[ \int_{T_n^-} (\nabla' \cdot \mathbf{f}_n) \mathbf{G}_0(\mathbf{r}, \mathbf{r}') dS' \right] dS \\ &\quad + j \frac{\eta}{k} \int_{T_m^-} (\nabla \cdot \mathbf{f}_m) \left[ \int_{T_n^+} (\nabla' \cdot \mathbf{f}_n) \mathbf{G}_0(\mathbf{r}, \mathbf{r}') dS' \right] dS. \end{aligned} \quad (6)$$

The surface divergence of the function  $f_n$ , which is proportional to the surface charge density, is

$$\nabla \cdot \mathbf{f}_n = \begin{cases} +\lambda_n / A_n^+ & \mathbf{r} \text{ in } T_n^+ \\ -\lambda_n / A_n^- & \mathbf{r} \text{ in } T_n^- \end{cases}, \quad (7)$$

where  $\lambda$  is the edge length and  $A$  is the area of the triangle. Using this property and defining

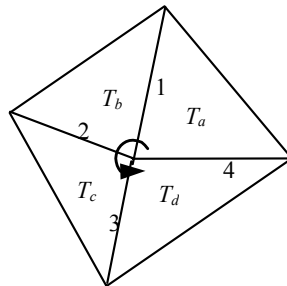
$$I(m^+, n^-) = \int_{T_m^+} \left[ \int_{T_n^-} \mathbf{G}_0(\mathbf{r}, \mathbf{r}') dS' \right] dS, \quad (8)$$

(6) can be written as

$$C_{2mn} = j \frac{\eta}{k} \begin{bmatrix} \left( \frac{\lambda_m}{A_m^+} \right) \left( \frac{\lambda_n}{A_n^+} \right) I(m^+, n^+) \\ + \left( -\frac{\lambda_m}{A_m^-} \right) \left( \frac{\lambda_n}{A_n^+} \right) I(m^-, n^+) \\ + \left( \frac{\lambda_m}{A_m^+} \right) \left( -\frac{\lambda_n}{A_n^-} \right) I(m^+, n^-) \\ + \left( -\frac{\lambda_m}{A_m^-} \right) \left( -\frac{\lambda_n}{A_n^-} \right) I(m^-, n^-) \end{bmatrix}. \quad (9)$$

Suppose an inner node is surrounded by 4 triangles,  $T_a$ ,  $T_b$ ,  $T_c$ , and  $T_d$  and the edges shared by these four triangles are edges 1, 2, 3, and 4 as shown in Fig. 1. For simplicity, the orientations of the edges are defined to be counterclockwise. Now consider the integrals for these observation edges and a source edge  $n$ , also shown in Fig. 1.

$$C_{21n} = j \frac{\eta}{k} \begin{bmatrix} \left( \frac{\lambda_1}{A_a} \right) \left( \frac{\lambda_n}{A_n^+} \right) I(a, n^+) \\ + \left( -\frac{\lambda_1}{A_b} \right) \left( \frac{\lambda_n}{A_n^+} \right) I(b, n^+) \\ + \left( \frac{\lambda_1}{A_a} \right) \left( -\frac{\lambda_n}{A_n^-} \right) I(a, n^-) \\ + \left( -\frac{\lambda_1}{A_b} \right) \left( -\frac{\lambda_n}{A_n^-} \right) I(b, n^-) \end{bmatrix}, \quad (10.a)$$



$$C_{22n} = j \frac{\eta}{k} \begin{bmatrix} \left( \frac{\lambda_2}{A_b} \right) \left( \frac{\lambda_n}{A_n^+} \right) I(b, n^+) \\ + \left( -\frac{\lambda_2}{A_c} \right) \left( \frac{\lambda_n}{A_n^+} \right) I(c, n^+) \\ + \left( \frac{\lambda_2}{A_b} \right) \left( -\frac{\lambda_n}{A_n^-} \right) I(b, n^-) \\ + \left( -\frac{\lambda_2}{A_c} \right) \left( -\frac{\lambda_n}{A_n^-} \right) I(c, n^-) \end{bmatrix}, \quad (10.b)$$

$$C_{23n} = j \frac{\eta}{k} \begin{bmatrix} \left( \frac{\lambda_3}{A_c} \right) \left( \frac{\lambda_n}{A_n^+} \right) I(c, n^+) \\ + \left( -\frac{\lambda_3}{A_d} \right) \left( \frac{\lambda_n}{A_n^+} \right) I(d, n^+) \\ + \left( \frac{\lambda_3}{A_c} \right) \left( -\frac{\lambda_n}{A_n^-} \right) I(c, n^-) \\ + \left( -\frac{\lambda_3}{A_d} \right) \left( -\frac{\lambda_n}{A_n^-} \right) I(d, n^-) \end{bmatrix}, \quad (10.c)$$

$$C_{24n} = j \frac{\eta}{k} \begin{bmatrix} \left( \frac{\lambda_4}{A_d} \right) \left( \frac{\lambda_n}{A_n^+} \right) I(d, n^+) \\ + \left( -\frac{\lambda_4}{A_a} \right) \left( \frac{\lambda_n}{A_n^+} \right) I(a, n^+) \\ + \left( \frac{\lambda_4}{A_d} \right) \left( -\frac{\lambda_n}{A_n^-} \right) I(d, n^-) \\ + \left( -\frac{\lambda_4}{A_a} \right) \left( -\frac{\lambda_n}{A_n^-} \right) I(a, n^-) \end{bmatrix}. \quad (10.d)$$

In (10),  $C_{2in}$  is the element on the  $i^{\text{th}}$  row and  $n^{\text{th}}$  column of  $\mathbf{C}_2$ . It is easy to show that these elements are dependent, and satisfy the following equation [8],

$$\frac{C_{21n}}{\lambda_1} + \frac{C_{22n}}{\lambda_2} + \frac{C_{23n}}{\lambda_3} + \frac{C_{24n}}{\lambda_4} = 0. \quad (11)$$

Since  $n$  can be any edge in the mesh, (11) indicates that rows 1, 2, 3, and 4 of  $\mathbf{C}_2$  are linearly

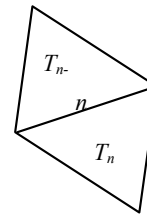


Figure 1. Source and observation triangles.



$\mathbf{C}_2$  in Equation (5) is singular if closed loops exist in the mesh. The rows forming a loop are linearly dependent as shown in (11) and we can write them in a form similar to (13),

$$\left(\frac{\mathbf{C}_{21}}{\lambda_1}\right) = (\pm a)\left(\frac{\mathbf{C}_{22}}{\lambda_2}\right) + (\pm b)\left(\frac{\mathbf{C}_{23}}{\lambda_3}\right) + (\pm c)\left(\frac{\mathbf{C}_{24}}{\lambda_4}\right) \quad (18)$$

where  $\frac{\mathbf{C}_{2i}}{\lambda_i}$  is the  $i^{\text{th}}$  row of  $\mathbf{C}_2$  normalized by the edge length. Comparing (18) to (11), it is clear that the coefficients  $a$ ,  $b$ , and  $c$  should be either 1 or  $-1$ . It is not difficult to rearrange the edges in the mesh so that the LU decomposition of  $\mathbf{C}_2$  can be written as in (15). If we fill (17) with the  $\mathbf{L}$  matrix and solve the equation, the solution  $\mathbf{R}$  should be a vector with integer elements. The non-zero integers correspond to edges forming a loop with one of the dependent edges, and zero values correspond to edges not related to the loop. The numerical solution will not be exact. However, it is accurate enough for us to identify all the integers. So we can determine the edges forming a loop and how they are related. Moreover, we can replace the elements in the solution with the exact values of the integers and recalculate  $\mathbf{L}_{di}$  using (17). This modification, together with the modification of  $\mathbf{U}$ , not only makes those rows dependent but also corrects their linear relation and recovers the scalar potential space.

In practice, we decompose  $\mathbf{C}_2$  in the form,

$$\mathbf{C}_2 = \mathbf{L} \cdot \mathbf{U} \cdot \mathbf{L}' \quad (19)$$

where  $\mathbf{L}$  is the lower triangular matrix resulting from an LU decomposition. Since  $\mathbf{C}_2$  is symmetric, the  $\mathbf{U}$  matrix in (19) is also symmetric and  $\mathbf{U}$  is still partitioned into four parts as in (15).  $\mathbf{U}$  can then be modified by setting  $\mathbf{U}_{di}$ ,  $\mathbf{U}_{id}$ , and  $\mathbf{U}_{dd}$  to zero. In this manner, we make all modifications symmetrically thus maintaining the symmetric property of the new  $\mathbf{C}_2$  matrix.

After the LU recombination, the errors in  $\mathbf{C}_2$  are eliminated and the information from  $\mathbf{C}_1$  is preserved. This can be seen from the equation below.

$$\begin{aligned} \mathbf{C} &= \mathbf{C}_1 + \mathbf{C}_2 = \mathbf{L}\mathbf{D}\mathbf{L}' + \mathbf{L}\mathbf{U}\mathbf{L}' \\ &= \mathbf{L} \left( \begin{bmatrix} \mathbf{D}_{ii} & \mathbf{D}_{id} \\ \mathbf{D}_{di} & \mathbf{D}_{dd} \end{bmatrix} + \begin{bmatrix} \mathbf{U}_{ii} & \mathbf{U}_{id} \\ \mathbf{U}_{di} & \mathbf{U}_{dd} \end{bmatrix} \right) \mathbf{L}', \end{aligned} \quad (20)$$

where  $\mathbf{L}$  and  $\mathbf{U}$  are the same as in (19).  $\mathbf{D}$  is a matrix such that  $\mathbf{C}_1 = \mathbf{L} \cdot \mathbf{D} \cdot \mathbf{L}'$ .  $\mathbf{U}_{di}$ ,  $\mathbf{U}_{id}$ , and  $\mathbf{U}_{dd}$  are set to zero in the recombination. Their counterparts,  $\mathbf{D}_{di}$ ,  $\mathbf{D}_{id}$ , and  $\mathbf{D}_{dd}$ , however, are so small that the new  $\mathbf{C}$  is still poorly conditioned when summing up  $\mathbf{D}$

and  $\mathbf{U}$ . In previously described loop-tree schemes, the frequency scaling property of the operators was analyzed and frequency normalization was applied to the elements of the EFIE matrix [5, 6]. In the modified LU recombination method we reduce the imbalance between the magnitudes of the matrix elements by scaling the vector potential part, that is, the sub matrices  $\mathbf{D}_{di}$ ,  $\mathbf{D}_{id}$ , and  $\mathbf{D}_{dd}$  in (20). This scaling is based directly on the magnitudes of the elements in  $\mathbf{C}_1$  and  $\mathbf{C}_2$  rather than on the frequency dependence. In our examples, this greatly improves the condition of the  $\mathbf{C}$  matrix.

#### IV. NUMERICAL RESULTS

We applied a boundary element method employing RWG basis functions, the LU recombination method, and the modified LU recombination method to the analysis of the square loop circuit shown in Figure 2. The circuit has a voltage source and a resistive load. The mesh has 74 edges and 10 inner nodes. Since the circuit itself is a loop, there are 11 loops in this mesh and there are 11 dependent rows in the  $\mathbf{C}_2$  matrix. Figure 3 shows the current through the load calculated by each of the three methods. Both the LU recombination method and the modified method calculate the current correctly down to frequencies as low as 1 Hz while the standard RWG method exhibits significant errors below 80 MHz.

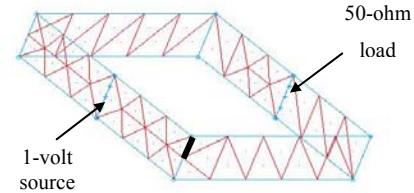


Figure 2. Mesh used to model a square loop circuit.

Figure 4 shows the current on another edge, indicated by the thick line in Figure 2. The current on this edge can be divided into two parts, one is the actual current flowing around the loop, and the other is an artificial current circling the inner node. The old LU recombination method exhibits errors below 10 kHz due to the artificial currents, but the modified method works well as low as 1 Hz.

Figure 5 shows a simple electric dipole antenna with a voltage source on the center edge. From the mesh we can see that the source edge is not part of any loop. Figure 6 compares this current through this edge calculated by the three methods. The LU recombination method fails for this example,

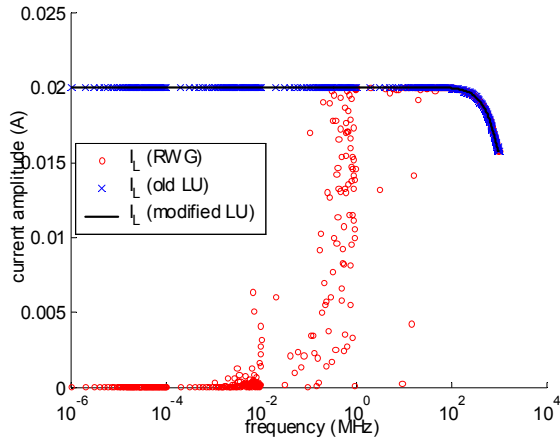


Figure 3. Current on the load edge of the loop circuit.

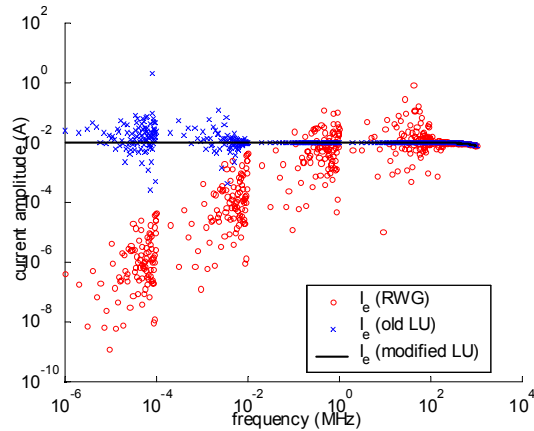


Figure 4. Current on a single edge of the loop circuit.

while both the standard RWG method and the modified method work fine. Figure 7 compares the current on another edge, indicated in Figure 5 by a thick line. In this case only the modified LU recombination method yields stable results below a few MHz.

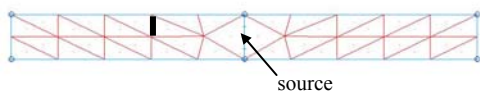


Figure 5. Mesh used to model a short dipole.

The dipole has a relatively simple mesh. We can readily observe how loops are formed around inner nodes in Figure 5, so it is relatively straightforward to implement the loop-tree scheme for this example. Figure 8 compares the current calculated by the modified LU recombination method to the current obtained using a loop-tree scheme. The results of the two methods match very well. The

unstable results at frequencies below 100 Hz are due to the significant imbalance in the scale of the vector and scalar potential terms. When we scale up the vector potential, the new method yields good results down to a few Hz, as shown in Figure 7.

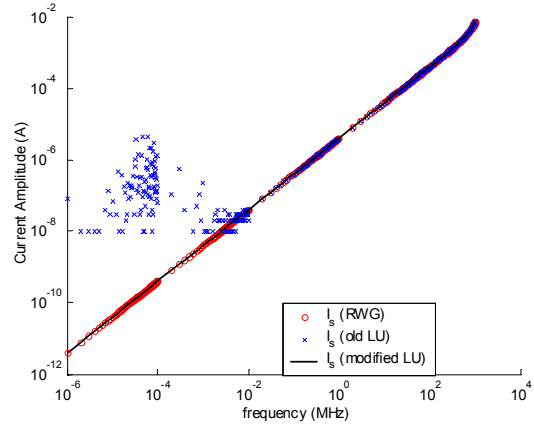


Figure 6. Current on the source edge of the dipole.

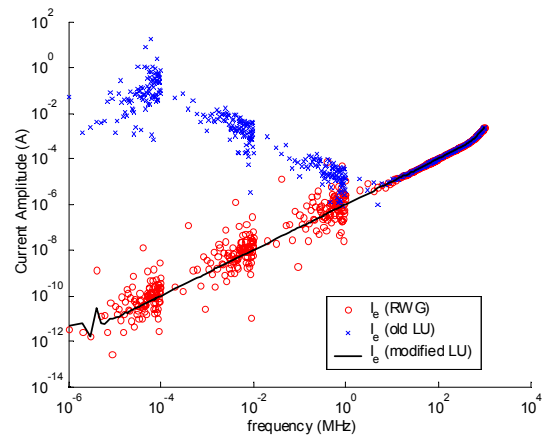


Figure 7. Current on a single edge of the dipole.

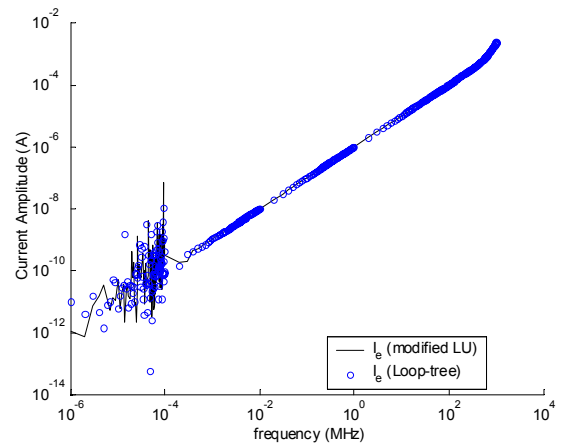


Figure 8. Modified LU and loop-tree results.

Figure 9 shows a simple circuit board configuration. Two traces of the same shape are centered over a 100-mm x 8-mm plate. The traces have the same length as the plate. They have a width of 1 mm and are placed 2 mm apart and 2 mm above the plate. One trace has a 1-volt source on one end and is terminated with a 50-ohm resistor. The other trace has 50-ohm resistors on both ends. Both the traces and the plate have zero thickness and are modeled as PEC surfaces. In order to observe conductive crosstalk at very low frequencies, a lumped resistance is located across the middle of the plate. The model employs 374 triangles and a total of 440 edges.

The current on the load resistor of the source trace, modeled using the RWG basis function method and the modified LU recombination method, is shown in Figure 10. Figure 11 shows the calculated current through the far-end resistor of the victim trace. In both cases, the standard RWG method exhibits significant errors below a few MHz, while the modified LU recombination method is accurate down to 1 Hz.

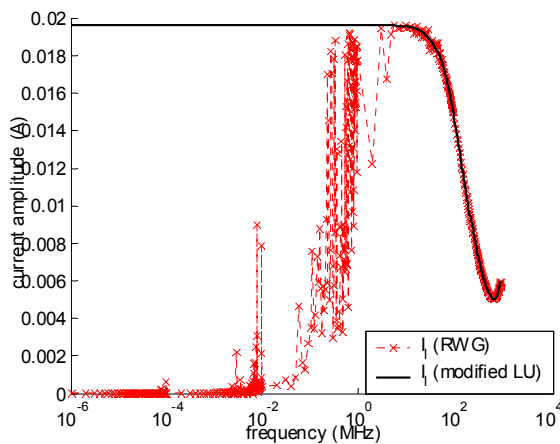


Figure 10. The current on the far end of the source trace.

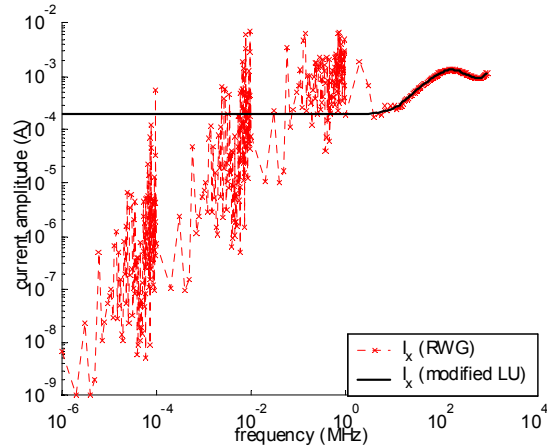


Figure 11. The coupled current on the far end of the victim trace.

### V. CONCLUSION

In this paper, a new method to remove the low frequency instability inherent in the boundary element method using RWG basis functions is presented. This method uses LU decomposition of the impedance matrix to find the dependent components in the integration of the scalar potential. It then recovers the correct relationship between the dependent components, by modifying the L and U matrices.

This method accomplishes the same goal as using loop-tree basis functions. However the new method extracts all the necessary information from the MoM matrix itself without requiring the user to define new basis functions. It enforces a zero scalar potential over closed loops and preserves the information from the vector potential that otherwise would be lost due to numerical error. Dipole and loop circuit examples demonstrate that this method is capable of working at frequencies as low as a few Hz.

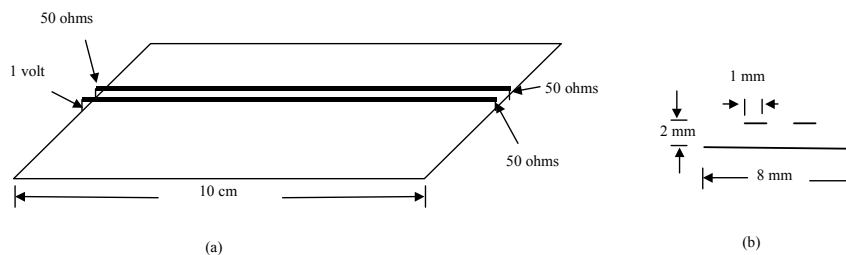
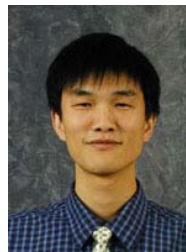


Figure 9. The crosstalk example. (a) geometry; (b) side view.

## REFERENCES

- [1] S. M. Rao, D. R. Wilton, and A. W. Glisson, "Electromagnetic scattering by surfaces of arbitrary shape," *IEEE Trans. Antennas Propagat.*, vol. AP-30, no. 3, pp. 409-418, May 1982.
- [2] M. Burton, S. Kashyap, "A study of a recent moment-method algorithm that is accurate to very low frequencies," *Appl. Computational Electromagn. Soc. J.*, vol. 10, no. 3, pp. 58-68, Nov. 1995.
- [3] W. Wu, A. W. Glisson, and D. Kajfez, "A study of two numerical solution procedures for the electric field integral equation at low frequency," *Appl. Comp. Electromagn. Soc. J.*, vol. 10, no. 3, pp. 69-80, Nov. 1995.
- [4] J. R. Mautz and R. F. Harrington, "An E-field solution for a conducting surface small or comparable to the wavelength," *IEEE Trans. Antennas Propagat.*, vol. AP-32, no. 4, pp. 330-339, Apr. 1984.
- [5] S. Y. Chen, W. C. Chew, J. M. Song, and J. S. Zhao, "Analysis of low frequency scattering from penetrable scatterers," *IEEE Trans. Geoscience and Remote sensing*, vol. 39, no. 4, pp. 726-735, Apr. 2001.
- [6] J. S. Zhao, W. C. Chew, "Integral equation solution of Maxwell's equations from zero frequency to microwave frequencies," *IEEE Trans. Antennas Propagat.*, vol. 48, no. 10, pp. 1635-1645, Oct. 2000.
- [7] Y. H. Zhang, T. J. Cui, W. C. Chew, and J. S. Zhao, "Magnetic field integral equation at very low frequencies," *IEEE Trans. Antennas Propagat.*, vol. 51, no. 8, pp. 1864-1871, Aug. 2003.
- [8] H. Ke and T. Hubing, "Using an LU Recombination Method to Improve the Performance of the Boundary Element Method at Very Low Frequencies," *Proc. of the 2005 IEEE Internat. Symp. on Electromagnetic Compatibility*, Chicago, USA, pp. 442-445, Aug. 2005.
- [9] A. Peterson, S. L. Ray, and R. Mittra, *Computational Methods for Electromagnetics*, Section 10.6, pp. 433-434, New York: IEEE Press, 1997.
- [10] Y. Ji, "Development and applications of a hybrid finite-element-method/method-of-moments (FEM/MOM) tool to model electromagnetic compatibility and signal integrity problems in printed circuit boards," Ph.D. dissertation, University of Missouri-Rolla, 2000.



**Haixin Ke** received his BSEE and MSEE degrees from Tsinghua University in 1998 and 2001, respectively. He is currently a Ph.D. student in Electrical Engineering at the University of Missouri-Rolla. His research interests include numerical modeling techniques for analyzing signal integrity and electromagnetic compatibility problems.



**Todd Hubing** received his BSEE degree from MIT in 1980, his MSEE degree from Purdue University in 1982, and his Ph.D. in Electrical Engineering from North Carolina State University in 1988.

From 1982 to 1989, he was an electromagnetic compatibility engineer for IBM in Research Triangle Park, NC. He is currently a Professor of Electrical and Computer Engineering at the University of Missouri-Rolla. He serves on the Board of Directors and is a Past President of the IEEE EMC Society.